ARMY RESEARCH LABORATORY

Time-Accurate Computations of Free-Flight Aerodynamics of a Spinning Projectile With and Without Flow Control

by Jubaraj Sahu

ARL-TR-3919 **September 2006**

Approved for public release; distribution is unlimited.

NOTICES

Disclaimers

The findings in this report are not to be construed as an official Department of the Army position unless so designated by other authorized documents.

Citation of manufacturer's or trade names does not constitute an official endorsement or approval of the use thereof.

DESTRUCTION NOTICE—Destroy this report when it is no longer needed. Do not return it to the originator.

Army Research Laboratory
Aberdeen Proving Ground, MD 21005-5066

ARL-TR-3919 **September 2006**

Time-Accurate Computations of Free-Flight Aerodynamics of a Spinning Projectile With and Without Flow Control

Jubaraj Sahu
Weapons and Materials Research Directorate, ARL

Approved for public release; distribution is unlimited.

REPORT DOCUMENTATION PAGE

Form Approved
OMB No. 0704-0188

Public reporting burden for this collection of information is estimated to average 1 hour per response, including the time for reviewing instructions, searching existing data sources, gathering and maintaining the data needed, and completing and reviewing the collection information. Send comments regarding this burden estimate or any other aspect of this collection of information, including suggestions for reducing the burden, to Department of Defense, Washington Headquarters Services, Directorate for Information Operations and Reports (0704-0188), 1215 Jefferson Davis Highway, Suite 1204, Arlington, VA 22202-4302. Respondents should be aware that notwithstanding any other provision of law, no person shall be subject to any penalty for failing to comply with a collection of information if it does not display a currently valid OMB control number.
PLEASE DO NOT RETURN YOUR FORM TO THE ABOVE ADDRESS.

1. REPORT DATE *(DD-MM-YYYY)* September 2006	**2. REPORT TYPE** Final	**3. DATES COVERED (From - To)** March 2005 to August 2006
4. TITLE AND SUBTITLE Time-Accurate Computations of Free-Flight Aerodynamics of a Spinning Projectile With and Without Flow Control		**5a. CONTRACT NUMBER** **5b. GRANT NUMBER** **5c. PROGRAM ELEMENT NUMBER**
6. AUTHOR(S) Jubaraj Sahu (ARL)		**5d. PROJECT NUMBER** 622618AH80 **5e. TASK NUMBER** **5f. WORK UNIT NUMBER**
7. PERFORMING ORGANIZATION NAME(S) AND ADDRESS(ES) U.S. Army Research Laboratory Weapons and Materials Research Directorate Aberdeen Proving Ground, MD 21005-5069		**8. PERFORMING ORGANIZATION REPORT NUMBER** ARL-TR-3919
9. SPONSORING/MONITORING AGENCY NAME(S) AND ADDRESS(ES)		**10. SPONSOR/MONITOR'S ACRONYM(S)** **11. SPONSOR/MONITOR'S REPORT NUMBER(S)**

12. DISTRIBUTION/AVAILABILITY STATEMENT

Approved for public release; distribution is unlimited.

13. SUPPLEMENTARY NOTES

14. ABSTRACT

This report describes a new multi-disciplinary computational study undertaken to compute the flight trajectories and simultaneously predict the unsteady free flight aerodynamics of a spinning projectile configuration with and without aerodynamic flow control. Actual flight trajectories are computed with an advanced coupled computational fluid dynamics (CFD)-rigid body dynamics (RBD) technique. An advanced time-accurate Navier-Stokes computational technique has been used in CFD to compute the unsteady aerodynamics associated with the free flight of the spinning projectile at subsonic speeds. Computed positions and orientations of the projectile have been compared with actual data measured from free flight tests and are found to be generally in good agreement. The same advanced coupled procedure has been used to compute the aerodynamics of the spinning projectile with flow control with the use of a synthetic microjet. Unsteady numerical results obtained from the coupled method show the flow field, the aerodynamic forces and moments, and the flight trajectories of the projectile.

15. SUBJECT TERMS

coupled CFD-RBD; flow control; projectile aerodynamics; time accurate

16. SECURITY CLASSIFICATION OF:			**17. LIMITATION OF ABSTRACT**	**18. NUMBER OF PAGES**	**19a. NAME OF RESPONSIBLE PERSON**
a. REPORT	**b. ABSTRACT**	**c. THIS PAGE**			Jubaraj Sahu
Unclassified	Unclassified	Unclassified	SAR	30	**19b. TELEPHONE NUMBER** (*Include area code*) 410-278-3707

Standard Form 298 (Rev. 8/98)
Prescribed by ANSI Std. Z39.18

Contents

List of Figures **iv**

Acknowledgments **v**

1. Introduction **1**

2. Solution Technique **3**

2.1 Dual Time Stepping....4

2.2 Unsteady Jet Boundary Condition....4

2.3 Hybrid RANS-LES Model....5

2.4 Grid Movement....6

2.5 Six-Degree-of-Freedom Coupling....6

3. Results and Discussion **7**

4. Summary and Conclusions **16**

5. References **18**

Distribution List **20**

List of Figures

Figure 1. Projectile geometry. 8
Figure 2. Aft end geometry showing the jet location. 8
Figure 3. Computational grid near the projectile. 9
Figure 4. Schematic showing the jet actuation in one spin cycle (view from the back of the projectile). 9
Figure 5. Computed particle traces colored by velocity, jet on, M = 0.39. 10
Figure 6. Computed velocity magnitudes at a given instant in time. 11
Figure 7. Comparison of computed roll angle, jet off. 11
Figure 8. Comparison of computed Euler pitch angle, jet off for different time steps. 12
Figure 9. Comparison of the computed Euler yaw angle, jet off for different time steps. 13
Figure 10. Comparison of the computed z distance, jet off. 13
Figure 11. Comparison of the computed y distance, jet off. 14
Figure 12. Comparison of the computed Euler pitch angle, LNS, jet off and jet on (jet velocity = 110 m/s). 15
Figure 13. Comparison of the computed side force and the normal force, LNS, jet off and jet on (jet velocity = 110 m/s). 15
Figure 14. Comparison of the computed y distance, LNS, jet off and jet on (jet velocity = 110 m/s). 16

Acknowledgments

This work was accomplished as part of a grand challenge project jointly sponsored by the Department of Defense High Performance Computing Modernization program and the U.S. Army Research Laboratory (ARL). The author wishes to thank Dr. Sukumar Chakravarthy of Metacomp Technologies for his technical assistance with some of the issues on the coupling techniques between computational fluid dynamics and rigid body dynamics. The author also wishes to thank Mr. Wayne Hathaway of Arrow Tech Associates for providing expert advice and helping with the six-degrees-of-freedom simulations with the software, ARFDAS (Aeroballistics Research Facility Data Analysis System). The scientific visualization and the computational support of ARL's Major Shared Resource Center are greatly appreciated.

INTENTIONALLY LEFT BLANK.

1. Introduction

The prediction of aerodynamic coefficients for projectile configurations is essential in the assessment of the performance of new designs. Accurate determination of aerodynamics is critical to the low-cost development of new, advanced guided projectiles, rockets, missiles, and smart munitions. Fins, canards, and jets can be used to provide control for maneuvering projectiles and missiles. The flow fields associated with these control mechanisms for the Army weapons are complex, involving three-dimensional (3-D) shock-boundary layer interactions, jet interaction with the free stream flow, and highly viscous dominated separated flow regions (*1, 2, 3*). The jet interference can extend over significant portions of the projectile and must be modeled correctly. For missiles, jet thrusters have been studied over a number of years to provide high-speed aerodynamic control. These thrusters interact with the surrounding flow field, and the resulting jet interaction flow field again is complex. Recently, several studies have shown that tiny synthetic unsteady jets can significantly alter the flow field and pressure distributions for airfoils and cylinders (*4, 5, 6*). These synthetic jets are active control devices with zero net mass flux and are intended to produce the desired control of the flow field through momentum effects. Many parameters such as jet location, jet velocity, and actuator frequency can affect the flow control phenomenon.

Smith and Glezer (*4*) have conducted an excellent study of the flow control by synthetic jets to provide increased fundamental understanding of the flow physics. Amitay et al. (5) experimentally investigated flow separation control on a cylinder using synthetic jet actuators. Their work showed that the interaction of the synthetic jet with the free stream flow resulted in a virtual modification of the body shape and significantly increased the lift force as a result of the flow reattachment. Aerodynamic flow control over an unconventional airfoil has also been demonstrated by Amitay et al. (*6*) to enhance post-stall performance with actuators operating at frequencies higher than the characteristic frequency of the airfoil. The synthetic jets are also being investigated for possible applications to improve heat transfer and drag reduction and to enhance mixing (*7*) in combustors, etc. The present analysis involves these synthetic jets for projectile aerodynamic control. The emphasis in the present research is to provide insight into the interaction of these unsteady jets with the free stream flow and to determine the feasibility of these jets for aerodynamic control of a subsonic spinning projectile. In addition, the objective was to accomplish it through coupled computational fluid dynamics (CFD) and rigid body dynamics (RBD) methods.

Computational and experimental data for these jet interactions are very limited. Simple theories cannot predict the complex flow fields associated with the jet interaction, and experimental tests are very expensive. To help reduce experimental costs, CFD is being used to predict these complex flows and provide detailed pressure, force, and moment data. There have been several recent numerical studies (*8, 9*) of flow separation control using synthetic jet actuators. He and

Kral (*8*) have used Reynolds-averaged Navier-Stokes (RANS) to study the effect of jet location and jet-forcing frequency on the lift and drag forces on an airfoil. The jet actuator was shown to increase the time-averaged lift and the amplitude of oscillation. Lee and Goldstein (*9*) have used the direct numerical simulation (DNS) on a two-dimensional synthetic jet. Although this simulation produced very good results, the use of DNS to model practical 3-D flows of interest is prohibitive because of its computing resources requirement. Even large eddy simulations (LES) (*10*) in which large eddies are computed directly and the small scales are modeled require large computational cost compared to RANS simulations. Although the RANS method works well for steady flows, the accuracy of this method for unsteady flows may be less than desired. Since the large energy-containing eddies are computed in the LES method, this technique is more capable of handling unsteady shear layers and wakes, etc. Recently, therefore, a hybrid approach (*11, 12*) that combines RANS and LES has been developed to solve practical problems of interest involving unsteady flows at reasonable computational cost. Both RANS and hybrid RANS-LES models have been used in the present study.

The advanced CFD capability used here solves the Navier-Stokes equations (*13 through 16*) and incorporates unsteady boundary conditions for the simulation of the synthetic jets (*17, 18*). Also, a hybrid RANS-LES turbulence model (*12*) was used for accurate numerical prediction of unsteady jet flows. Sahu (*19*) used these advanced techniques and performed numerical flow field computations for steady and unsteady jets for a non-spinning projectile configuration at a low subsonic speed. Computed lift forces attributable to the unsteady synthetic jets were found to match well the experimental data (*17, 18*). That research work was further extended to a spinning projectile at subsonic speeds (*20*). Results obtained for the spinning projectile configuration were reported at Mach 0.24, angle of attack 0 degrees and a spin rate of 67 Hz.

The present numerical study is a big step forward and a direct extension of that research which now includes numerical simulation of the actual flight paths of the projectile with and without flow control using coupled CFD-RBD techniques. The present research allows “virtual fly-out” of projectiles on the supercomputers and allows numerical prediction of the actual flight paths of a projectile and all the associated unsteady free flight aerodynamics using coupled CFD-RBD techniques in an integrated manner. Sahu (*21*) has successfully applied such advanced coupled procedures to simultaneously determine the flight trajectory and the associated unsteady free-flight aerodynamics of a finned projectile at supersonic velocity. The present research is an extension of this work to a spinning projectile at a subsonic speed with and without flow control. The following sections describe the coupled numerical procedure and the computed results obtained for the spinning body of revolution at subsonic speeds.

2. Solution Technique

At the U.S. Army Research Laboratory (ARL), research efforts are performing real-time multidisciplinary-coupled CFD-RBD aerodynamic computations for the entire flight trajectory of a complex guided projectile system. A real-time accurate approach is used in the present work; however, the computations require much greater computer resources. The real-time accurate approach requires that the six-degrees-of-freedom (6-DOF) body dynamics be computed at each repetition of a flow solver. The CFD capability used here solves the Navier-Stokes equations and incorporates advanced boundary conditions and grid motion capabilities. The complete set of 3-D time-dependent Navier-Stokes equations is solved in a time-accurate manner for simulations of actual flights. A commercially available code, CFD++ (*17, 18, 19, 20*), is used for the time-accurate unsteady CFD simulations. The basic numerical framework in the code contains unified grid, unified physics, and unified computing features. The user is referred to these references for details of the basic numerical framework.

The 3-D, time-dependent RANS equations are solved by the following finite volume method:

$$\frac{\partial}{\partial t}\int_V \mathbf{W}dV + \oint[\mathbf{F}-\mathbf{G}]\cdot dA = \int_V \mathbf{H}dV \tag{1}$$

in which **W** is the vector of conservative variables, **F** and **G** are the inviscid and viscous flux vectors, respectively, **H** is the vector of source terms, V is the cell volume, and A is the surface area of the cell face.

For low speed flows considered here, the "preconditioned implicit relaxation" scheme is used to achieve faster convergence. It combines three basic ideas: (a) implicit local time stepping, (b) relaxation, and (c) preconditioning. Preconditioning the equations ideally equalizes the eigenvalues of the inviscid flux Jacobians and removes the stiffness arising from large discrepancies between the flow and sound velocities at low speeds. The use of an implicit scheme circumvents the stringent stability limits suffered by their explicit counterparts, and successive relaxation allows cells to be revised as information becomes available and thus aids convergence. These features of the code have been extremely useful in the present numerical simulations at very low subsonic speeds. Second order discretization was used for the flow variables and the turbulent viscosity equation. The turbulence closure is based on topology-parameter-free formulations. Two-equation and higher order hybrid RANS-LES turbulence models were used to compute turbulent flows. These models are ideally suited to unstructured bookkeeping and massively parallel processing because of their independence from constraints related to the placement of boundaries and/or zonal interfaces.

For computations of unsteady jet interaction flow fields that are of interest here, dual time stepping as described next was used to achieve the desired time accuracy. In addition, special jet boundary conditions were developed and used for the numerical modeling of synthetic jets. Grid was actually moved to take into account the spinning motion of the projectile.

2.1 Dual Time Stepping

The "dual time-stepping mode" of the code was used to perform the transient flow simulations. The term "dual time step" implies the use of two time steps. The first is an "outer" or global (and physical) time step that corresponds to the time discretization of the physical time variation term. This time step can be chosen directly by the user and is typically set to a value to represent 1/100 of the period of oscillation expected or forced in the transient flow. It is also applied to every cell and is not spatially varying.

An artificial or "inner" or "local" time variation term is added to the basic physical equations. This time step and corresponding "inner iteration" strategy is chosen to help satisfy the physical transient equations to the desired degree. If the inner iterations converge, then the outer physical transient equations (or their discretization) are satisfied exactly; otherwise, they are satisfied approximately. For the inner iterations, the time step is allowed to vary spatially. Also, relaxation with multi-grid (algebraic) acceleration is employed to reduce the residues of the physical transient equations. It is found that an order of magnitude reduction in the residues is usually sufficient to produce a good transient iteration. This may require a few internal iterations (between 5 and 10) to achieve, depending on the magnitude of the outer time step, the nature of the problem, the nature of the boundary conditions, and the consistency of the mesh with respect to the physics at hand.

2.2 Unsteady Jet Boundary Condition

A large number of boundary conditions (BC) are available and can be specified at the appropriate boundaries. Each BC is encoded as a basic form along with a collection of modifiers. One particular BC used for the simulations presented here is an "oscillating jet" BC. In its basic form, it is a steady inflow/outflow BC wherein the user supplies the velocity normal to the boundary along with static temperature and any turbulence quantities. When the velocity provided is negative, it is considered to be an inflow and when it is positive, it is treated as an outflow. In the case of inflow, the static temperature and turbulence quantities are used, along with the inflow velocity. In the case of outflow, only the velocity is used. At inflow, the tangential component of velocity is set to zero and at outflow, the tangential component is extrapolated from the interior. At outflow, all primitive variables except normal velocity are extrapolated from the interior. At inflow, the static pressure is taken from the interior.

The first modifier available for this BC allows the velocity to oscillate. The base velocity is multiplied by an amplitude that varies as sin ($2\pi ft$) where f is the frequency of the oscillation.

Thus, the oscillating velocity can cycle from being positive to being negative and back within each period (or from being negative to positive and back, based on the sign of the input for the basic BC formulation).

A second modifier permits the steady or oscillating inflow/outflow to be on during certain time intervals and off during other intervals. During "on" periods, the basic or the basic multiplied by the oscillating amplitude multiplier (first modifier) is used. The user provides the ranges of time during which the jet is on. The user also provides a repetition time period (e.g., the time period corresponding to one spin rotation of the projectile). Within each time period, therefore, there are sets of starting and ending times, which define when the jet is on. During "off" periods, the amplitude is set to zero. In parts of the cycle when the jet is off, the boundary condition thus reverts to the condition of inviscid surface tangency. This procedure allows the flow to slip past the boundary, as would exist (in the form of a shear layer) if the jet were emanating from a cavity or hole.

2.3 Hybrid RANS-LES Model

Currently, the two most popular forms of turbulence closure, namely, ensemble-averaged models (typically based on the RANS equations), and LES with a sub-grid-scale model, face a number of unresolved difficulties. Specifically, existing LES models have met with problems related to the accurate resolution of the near-wall turbulent stresses. In the near-wall region, the foundations of large-eddy simulation are less secure since the sizes of the (anisotropic) near-wall eddies approach those of the Kolmogorov scale, requiring a mesh resolution approaching that of a direct numerical simulation. On the other hand, existing ensemble-averaged turbulence models are limited by their empirical calibration. Their representation of small-scale flow physics cannot be improved if we refine the mesh, and over short time scales, they tend to be overly dissipative with respect to perturbations around the mean, often suppressing unsteady motion altogether.

Although LES is an increasingly powerful tool for unsteady turbulent flow prediction, it is still prohibitively expensive. To bring LES closer to becoming a design tool, a hybrid RANS-LES approach based on limited numerical scales (LNS) has been recently developed by Metacomp Technologies (*12*). This approach combines the best features of RANS and LES in a single modeling framework. The LNS model is formulated from an algebraic or differential Reynolds-stress model, in which the sub-grid stresses are limited by the numerically computed local length scale and velocity scale products. LNS thus behaves like its parent RANS model on RANS-type grids but reverts to an *anisotropic* LES sub-grid model as the mesh is refined locally, thereby reaching the correct (DNS) fine grid limit. Locally embedded regions of LES may be achieved automatically through local grid refinement, while the superior near-wall stress predictions of the RANS model are preserved, removing the need of *ad hoc*, topography-parameter-based wall damping.

The LNS hybrid formulation is well suited to the simulation of unsteady flows, including mixing flows, and contains no additional empirical constants beyond those appearing in the original RANS and LES sub-grid models. With this method, a regular RANS-type grid is used except in isolated flow regions where denser, LES-type mesh is used to resolve critical unsteady flow features. The hybrid model transitions smoothly between an LES calculation and a cubic k-ε model, depending on grid fineness. A somewhat finer grid was placed around the body and near the jet, the rest of the flow field being occupied by a coarser, RANS-like mesh.

To date, the LNS technique has been used successfully on a number of unsteady flows. Examples include flows over cavities, flows around blunt bodies, flows around airfoils and wings at high angle of attack, separation suppression using synthetic jets, forced and natural convection flows in a room, and mixing flows in nozzles. For computations of unsteady synthetic jet interaction flow fields that are of interest here, the hybrid RANS-LES or LNS technique was found to be essential in the accurate numerical predictions of such flows (*19, 20*).

2.4 Grid Movement

Grid velocity is assigned to each mesh point. This general capability can be tailored for many specific situations. For example, the grid point velocities can be specified to correspond to a spinning projectile. In this case, the grid speeds are assigned as if the grid is attached to the projectile and spinning with it. Similarly, to account for RBD, the grid point velocities can be set as if the grid is attached to the rigid body with 6 DOF. For the RBD, the coupling refers to the interaction between the aerodynamic forces and moments and the dynamic response of the projectile or body to these forces and moments. The forces and moments are computed every CFD time step and transferred to a 6-DOF module that computes the body's response to the forces and moments. The response is converted into translational and rotational accelerations that are integrated to obtain translational and rotational velocities and integrated once more to obtain linear position and angular orientation. The 6-DOF RBD module uses quaternions to define the angular orientations. However, these are easily translated into Euler angles. From the dynamic response, the grid point locations and grid point velocities are set.

2.5 Six-Degree-of-Freedom Coupling

In CFD++, two modes are available to help simulate RBD: an uncoupled mode and a coupled mode. The coupling refers to the interaction between the aerodynamic forces and moments and the dynamic response of the projectile or body to these forces and moments. In both modes, the forces and moments are computed every time step and reported to the user. In the coupled mode, the forces and moments are passed to a 6-DOF module which computes the body's response to the forces and moments. The response is converted into translational and rotational accelerations which are integrated to result in translational and rotational velocities and integrated once more to result in linear position and angular orientation. The 6-DOF RBD module uses quaternions to define the angular orientations. However, these are easily translated into Euler angles. From the

dynamic response, the grid point locations and grid point velocities are set. In the uncoupled mode, the forces and moments are not coupled with the RBD module. The motion of the projectile is kinematics only and depends on the initial linear and angular velocities prescribed.

Typically, we begin with a computation performed in "steady state mode" with the grid velocities prescribed to account only for the translational motion component of the complete set of initial conditions to be prescribed. At this stage, we also impose the angular orientations from the initial conditions. The complete set of initial conditions includes translational and rotational velocity components, along with initial position and angular orientation. With a fixed translational velocity, we obtain the steady state solution. This becomes the initial condition for the next step which involves adding just the spin component of the projectile. With the addition of spin, time-accurate calculations are performed for a few cycles of spin until converged periodic forces and moments are obtained. A sufficient number of time steps are performed so that the angular orientation for the spin axis corresponds to the prescribed initial conditions. All this is performed in an uncoupled mode. The angular velocity initial conditions associated with the non-spin rotational modes are then added. The mesh is translated back to the desired initial position, the non-spin rotational velocity initial conditions are turned on, and computations are performed in the coupled mode.

3. Results and Discussion

Time-accurate unsteady numerical computations were performed with Navier-Stokes and coupled 6-DOF methods to predict the flow field and aerodynamic coefficients and the flight paths of a subsonic spin-stabilized projectile for both jet-off and jet-on conditions at a subsonic speed, M = 0.39. The preconditioned version of the CFD++ code was used to obtain efficient numerical solution at low speed. For modeling of the unsteady synthetic jets, both unsteady RANS and a hybrid RANS-LES approach (*12*) were used. In all cases, full 3-D computations were performed and no symmetry was used.

The subsonic projectile is a 1.8-caliber ogive-cylinder configuration (see figure 1). Here, the primary interest is in the development and application of CFD-RBD techniques for accurate simulation of projectile flow field with and without flow control using unsteady microjets.

The first step here was to obtain the steady state results for the same projectile without the jet with the grid velocities prescribed. Also imposed were the angular orientations at this stage. Corresponding converged jet-off steady state solution was then used as the starting condition, along with the other initial conditions for the computation of coupled CFD-RBD runs. Synthetic jets were activated at a specified point in the trajectory. The jet locations on the projectile are shown in figure 2. The jet conditions were specified at the exit of the jet (sinusoidal variation in jet velocity). The jet conditions specified include the jet pressure, density, and velocity components.

The flow field inside the tiny jet cavity is not computed. For the unsteady jets, time-dependent jet boundary conditions are applied at the jet exit. Numerical computations have been made for these jet cases at an initial Mach number, M = 0.39, initial angle of attack, $\alpha = 2$ degrees, and an initial spin rate of 434 Hz. The jet width was 0.32 mm, the jet slot half-angle was 18 degrees, and the peak jet velocity used was 110 m/s operating at a frequency of 1000 Hz. The jet-off coupled calculations are started from the same initial conditions.

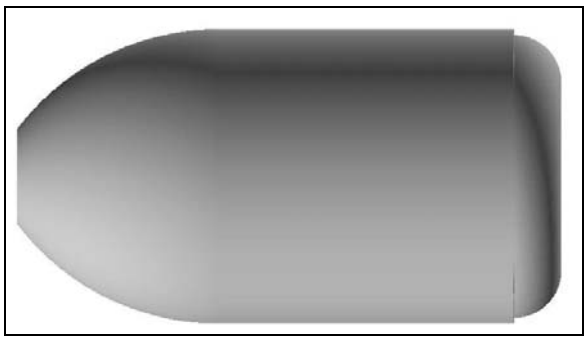

Figure 1. Projectile geometry.

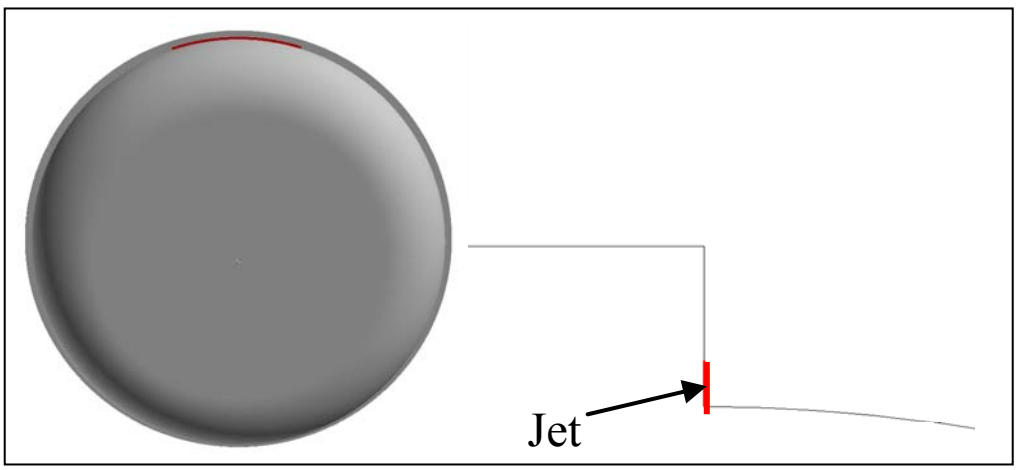

Figure 2. Aft end geometry showing the jet location.

A computational grid expanded near the vicinity of the projectile is shown in figure 3. Grid points are clustered near the jet as well as the boundary layer regions to capture the high gradients flow regions. The computational grid has 211 points in the streamwise direction, 241 in the circumferential direction, and 80 in the normal direction. The unsteady coupled numerical simulations took thousands of hours of central processing unit time on an IBM SP[1] P4 computer running with 32 to 64 processors.

Unsteady time-accurate CFD computations require huge computer resources. All the results presented here were obtained from unsteady numerical computations with a single synthetic jet on a 40-mm subsonic grenade (see figure 1). Looking from the back of the projectile (see figure 4),

[1]Not an acronym

we see that the projectile spins clockwise. The jet actuation corresponds to one-fourth of the spin cycle from -45 to +45 degrees with 0 degree being the positive y axis. The jet is off during the remaining three-fourths of the spin cycle. The unsteady CFD modeling technique required about 180 time steps to resolve a full spin cycle. The unsteady synthetic jet operates at a high frequency of 1000 Hz. For the part of the spin cycle when the jet is on, the jet operated for approximately four cycles.

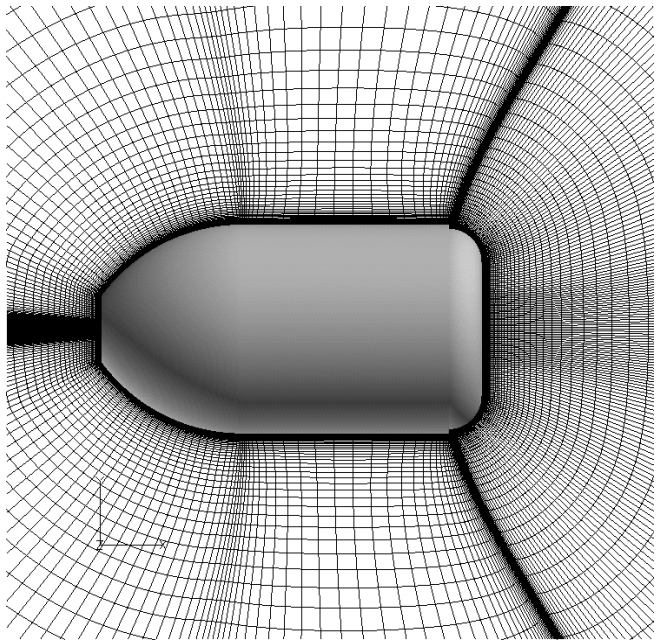

Figure 3. Computational grid near the projectile.

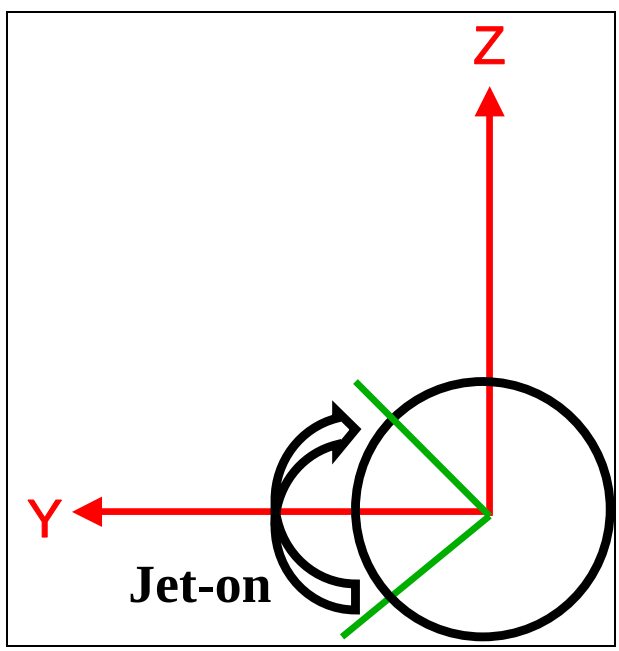

Figure 4. Schematic showing the jet actuation in one spin cycle (view from the back of the projectile).

Computed particle traces emanating from the jet into the wake are shown in figure 5 at a given instant in time for Mach = 0.39. These traces are colored by the velocity magnitude. The particle traces emanating from the jet interact with the wake flow, making it highly unsteady. It shows the flow in the base region to be asymmetric because of the interaction of the unsteady jet. The shear layer from the free stream flow resulting from the step corner up stream from the base interacts with the unsteady jet and breaks down just a short distance down stream from the jet. The unsteady jet substantially alters the flow field near the jet and the base region that in turn affected the forces and moments even at 0 degree angle of attack.

Figure 6 shows the velocity magnitude contours at a given time or at a given location in the trajectory. It clearly shows the orientation of the body at that instant in time and the resulting asymmetric flow field in the wake because of the body at angle of attack. The orientation of the projectile of course changes from one instant in time to another as the projectile flies down range. This includes the Euler pitch and yaw angles as well. The computed surface pressures from the unsteady dynamic flow fields are integrated to obtain the aerodynamic forces and moments. Computed results have been obtained with unsteady RANS (URANS) as well as the hybrid RANS-LES approach referred here as the LNS for the jet-on conditions. The unsteady jet is applied while the projectile is spinning (see figure 4). As pointed out earlier, the jet-off computa-tions have been made in a time-accurate dynamic coupled mode. Numerical calculations with the microjet are also computed with the coupled approach. Computational results for the jet-off case obtained with the coupled procedure are shown next. For these coupled simulations, the aerody-namic forces and moments were completely obtained through CFD as the projectile flew. The simulation started from the first station away from the muzzle where the actual data were measured. The first station was situated about 4.9 m from the muzzle.

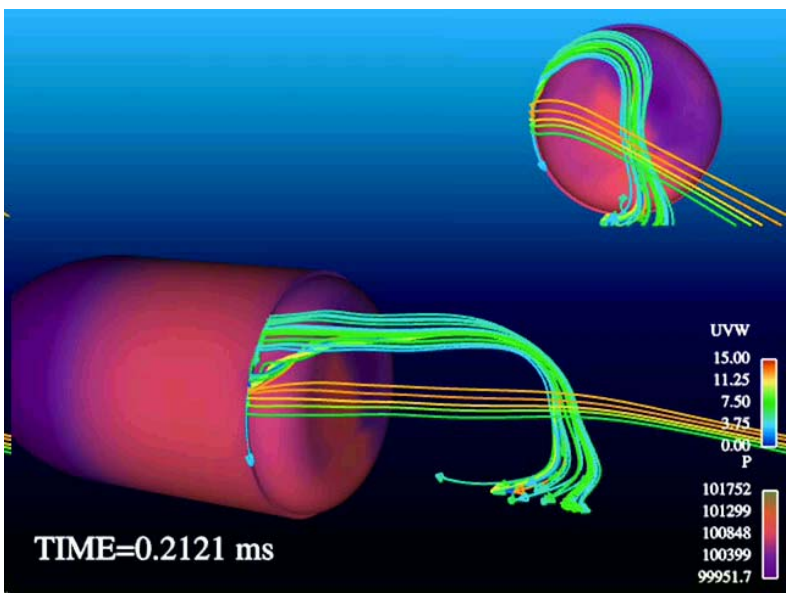

Figure 5. Computed particle traces colored by velocity, jet on, M = 0.39.

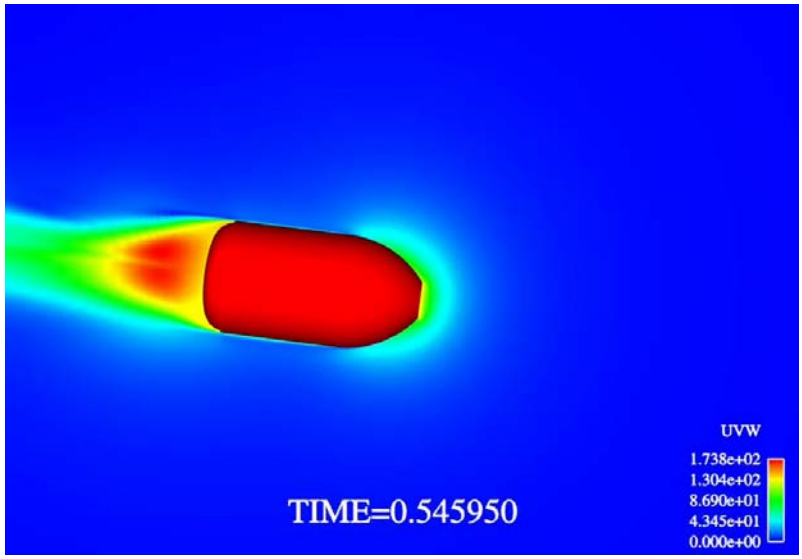

Figure 6. Computed velocity magnitudes at a given instant in time.

Figure 7 shows the computed roll angles as a function of the x-distance or the range. The roll angles shown here are the accumulated values to include 360 degrees for every spin cycle of the projectile. Computed roll angles are compared with the experimentally observed values as well as data obtained from the 6-DOF analysis of the flight results from ARFDAS (*22*) and are found to be in good agreement.

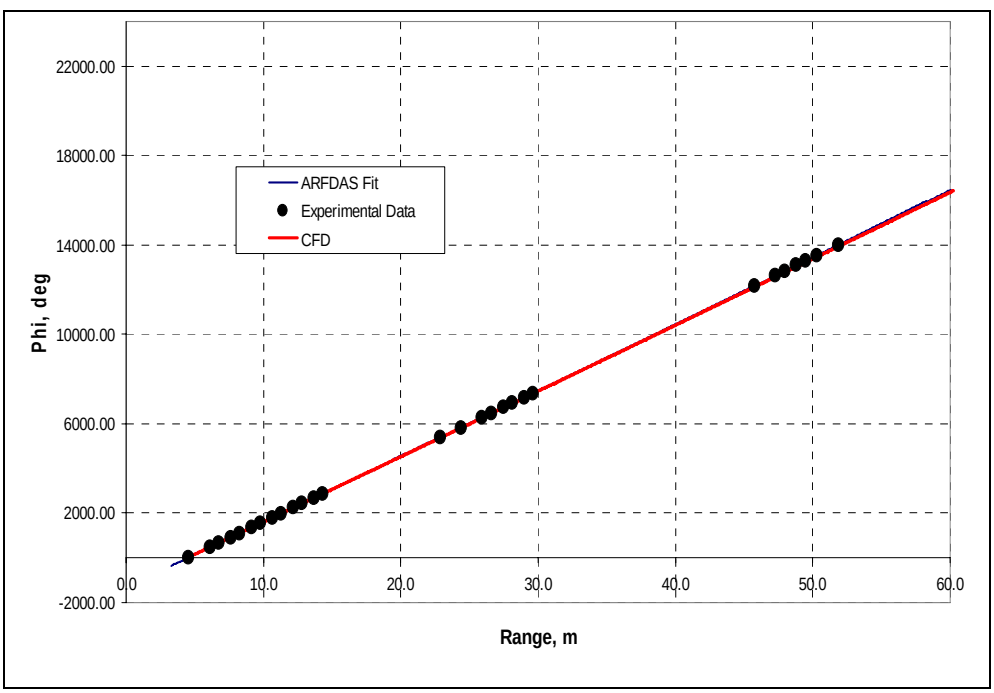

Figure 7. Comparison of computed roll angle, jet off.

Figure 8 shows the variation of the Euler pitch angle with distance traveled. As seen in this figure, both the amplitude and frequency in the Euler pitch angle variation are predicted very well by the computed results and match well with the data from the flight tests for a distance as far as 20 meters. For the rest of the trajectory, the frequency of the motion is predicted very well, as seen by the comparison with the data, but the amplitude does not compare as well with the data. Two sets of CFD results are shown in this figure, one set obtained with the original time step and another one with a smaller time step reduced by half from the original time step. As seen in this figure, reducing the time step by half has a negligible effect on the accuracy of the computed results. Figure 9 shows similar behavior with Euler yaw angle with x distance. The agreement between the computed results and the experimental data again is generally good except for the amplitude comparison at greater ranges. In figures 8 and 9, we have slow and fast mode frequencies and both compare well with the data and the ARFDAS fits.

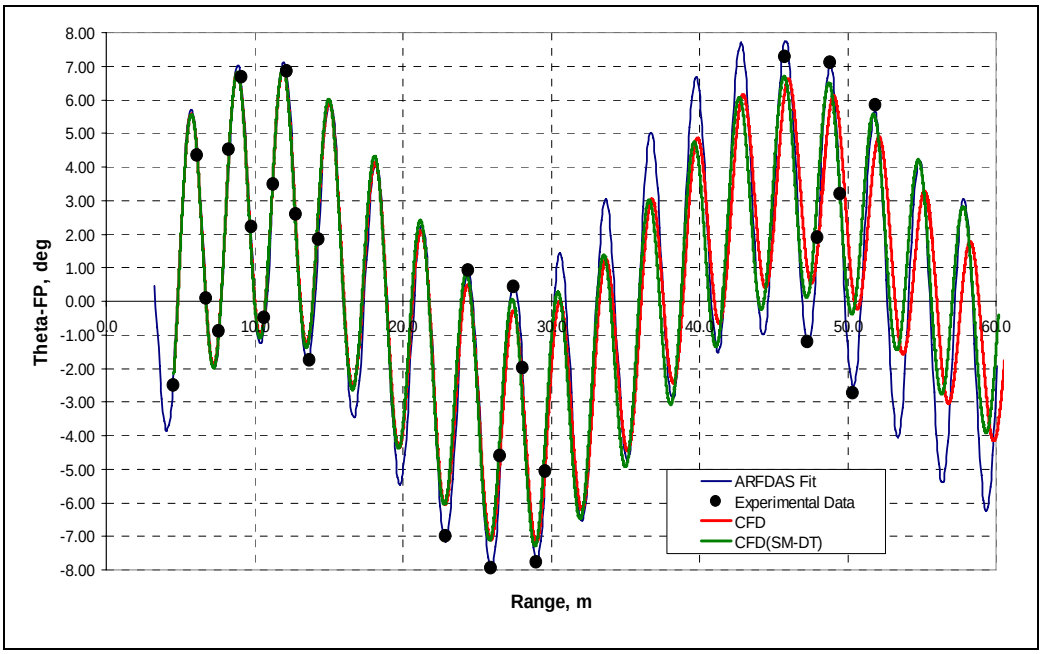

Figure 8. Comparison of computed Euler pitch angle, jet off for different time steps.

Figures 10 and 11 show the computed z and y distances, respectively, as a function of the x distance or range. Computed y and z distances were obtained with two different time steps (DT) of 0.00007875 and 0.00002625 and are compared with the actual measured data and the fits obtained through ARFDAS fits. The effect of time step on the computed y and z distances are very small, indicating that the smaller time step is good enough to provide the desired time accuracy. As shown in figure 10, the computed z distance compares very well with the data obtained from the flight test. The computed y distance is shown in figure 11. As can be seen, the computed y distance matches very well with the data in the early part of the trajectory, i.e., until about 30 m. The comparison of the computed result with the data is not so good for the rest of the trajectory. This small discrepancy can be attributed to errors in the computational geometric

modeling of the actual flight body, which can result in small differences in the prediction of the side force and Magnus moment for a spinning body, especially at a low subsonic speed. Additional research in these areas can possibly further improve the accuracy of the computed results. Although not shown here, the effect of inner time step iterarions was also studied and a calculation with 10 inner iterations yielded essentially the same results as were obtained with five sub-iterations.

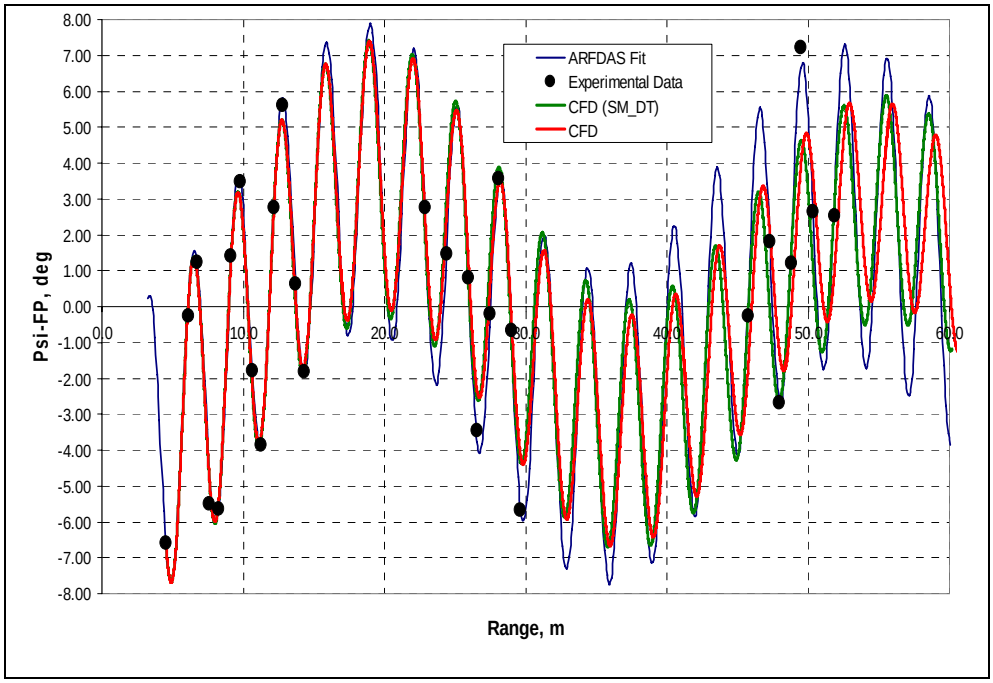

Figure 9. Comparison of the computed Euler yaw angle, jet off for different time steps.

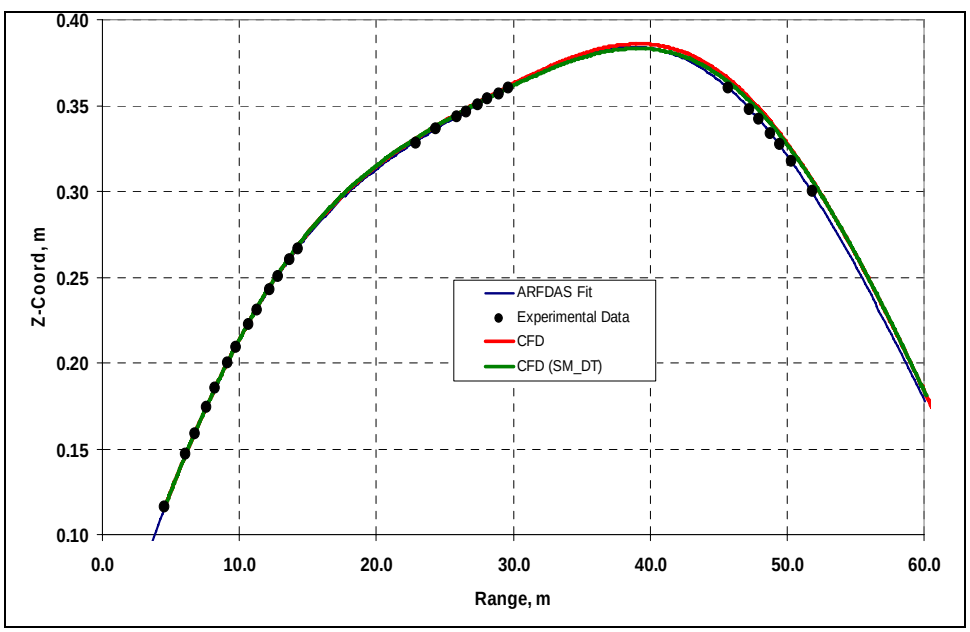

Figure 10. Comparison of the computed z distance, jet off.

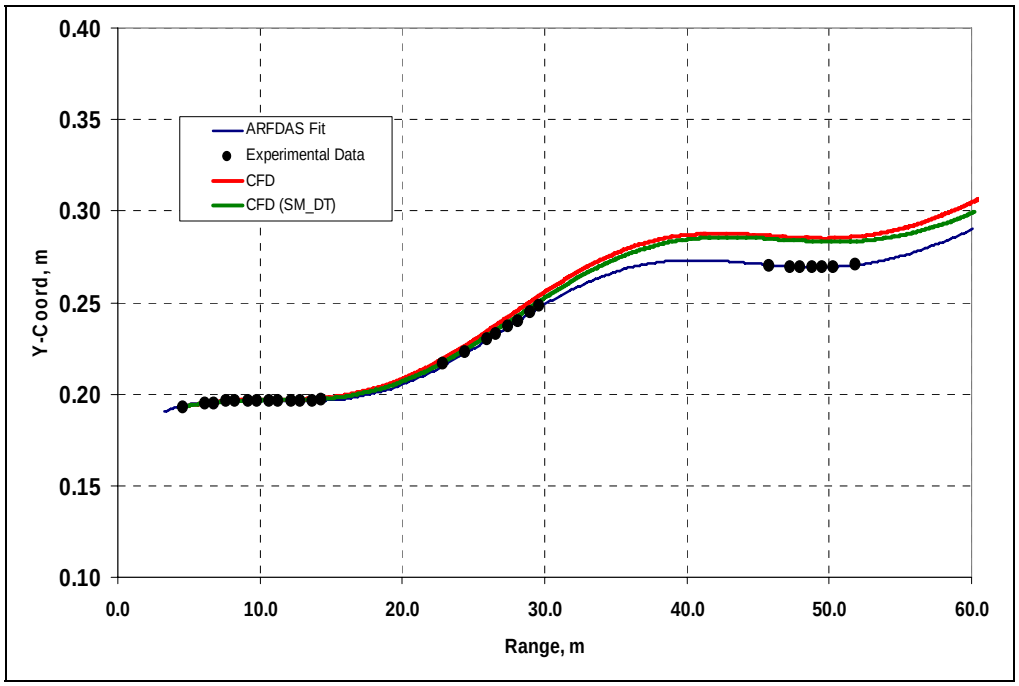

Figure 11. Comparison of the computed y distance, jet off.

A few results obtained for the spinning projectile with flow control are presented next. The unsteady synthetic microjet is applied while the projectile is spinning (see figure 4) so as to get a side force in this case. The synthetic jet was activated at approximately 41 meters into the trajectory. Figure 12 shows the variation of the Euler pitch angle with distance traveled. As seen in this figure, the effect of the jet obtained with the hybrid RANS-LES (or LNS) model is small. As seen here, the computed data with and without flow control are very similar. There is very little change in the frequency. However, small changes between the jet-off and jet-on results can be observed in the amplitude variations. Figure 13 shows the axial force (Fx), side force (Fy), and the lift or normal force (Fz) obtained with the LNS model as a function of the range. The effect of the jet is seen to increase the side force; however, the effect of the jet on the lift force is almost negligible. There is some effect on the axial force as well. Our primary interest is the effect of the unsteady microjet on the side force. Although only a small change is observed between the jet-off and jet-on results, it is expected that the cumulative effect of these changes over many spin cycles of the spinning body, i.e., across a larger x distance can be sufficient to provide the required control force for changing the course of the trajectory.

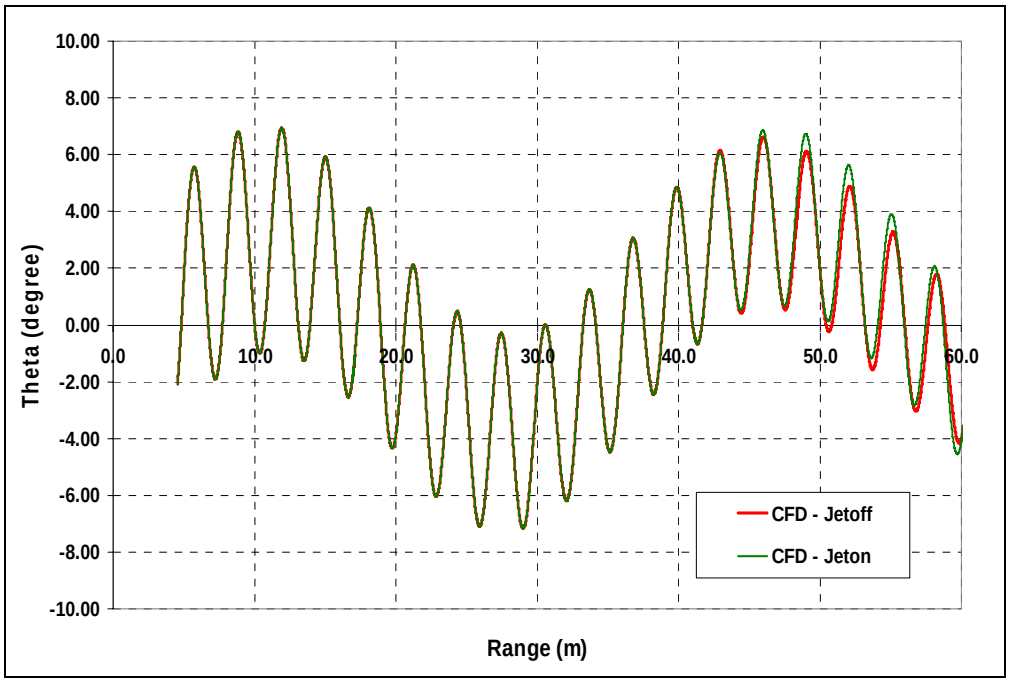

Figure 12. Comparison of the computed Euler pitch angle, LNS, jet off and jet on (jet velocity = 110 m/s).

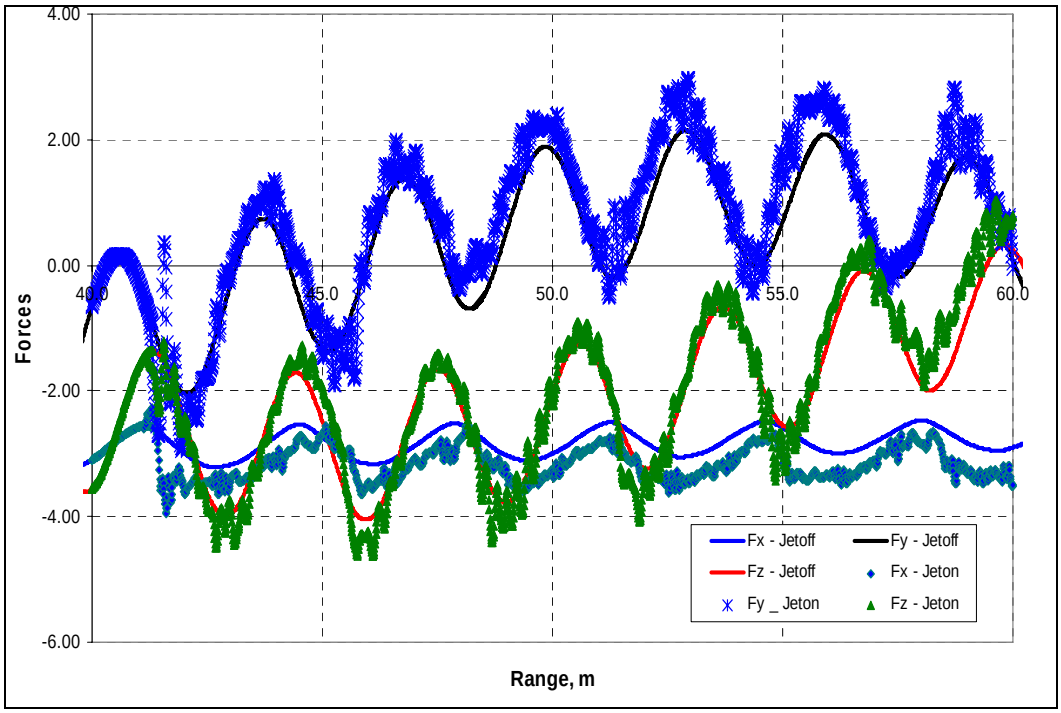

Figure 13. Comparison of the computed side force and the normal force, LNS, jet off and jet on (jet velocity = 110 m/s).

Figure 14 shows the variation of y distance as function of the range for both jet-off and jet-on conditions. Here, the jet-on results shown were obtained with the LNS approach. In addition, the jet-on computations were performed for many more spin cycles or for a greater range. One can clearly see the effect of the jet in the y distance; it increases with an increase in the range. These computed results strongly indicate that applying the jet in the positive y direction moves the projectile in the same positive direction with little or no effect on the other aerodynamic forces.

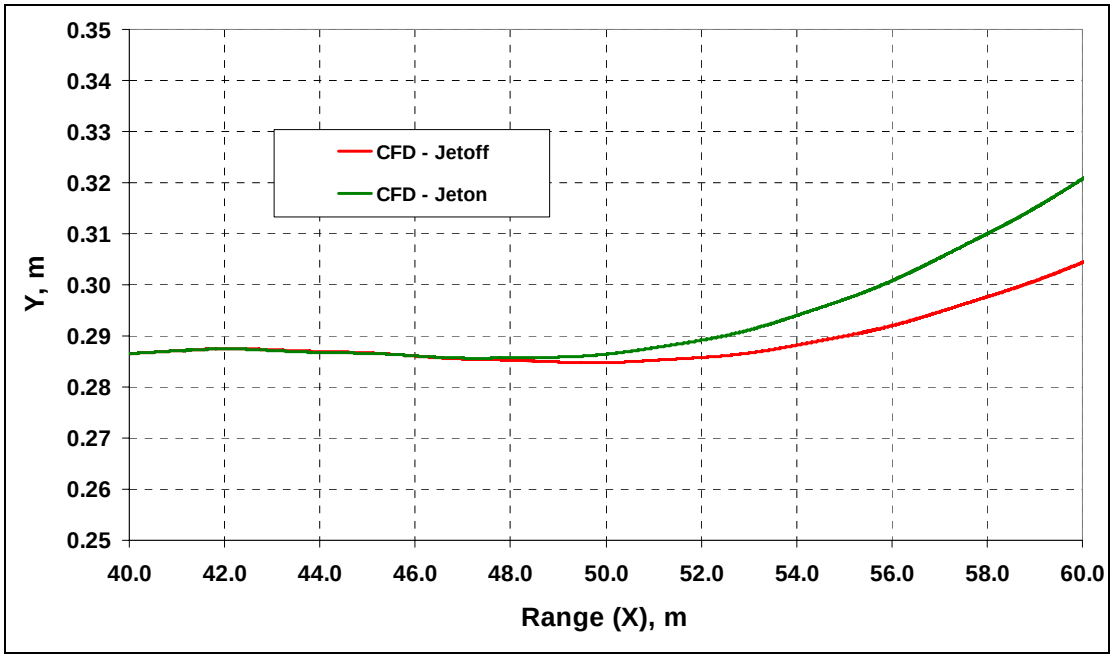

Figure 14. Comparison of the computed y distance, LNS, jet off and jet on (jet velocity = 110 m/s).

4. Summary and Conclusions

This report describes a new coupled CFD-RBD computational study undertaken to simultaneously determine the flight trajectory and the associated unsteady free-flight aerodynamics of a spinning projectile with and without flow control. A 3-D unsteady Navier-Stokes solver is employed to compute the time-accurate aerodynamics associated with the free flight of the spinning projectile at a low subsonic velocitiy. Computed results have been obtained at an initial low subsonic speed, M = 0.39 and α = 2 degrees for the spinning projectile with the use of the time-accurate Navier-Stokes computational technique and advanced turbulence models. Computed positions and orientations of the projectile have been compared with actual data measured from free-flight tests and are found to be generally in good agreement. The same advanced coupled procedure has been used to compute the aerodynamics of the spinning projectile with flow control using a synthetic

microjet. These computations with flow control clearly show the effect of the unsteady microjet on the side aerodynamic force.

This work demonstrates a coupled method to accurately predict the time-accurate unsteady aerodynamics of a spinning projectile. Computational results obtained with flow control show the potential of tiny microjets as a means to provide the control authority to maneuver a spinning projectile at low subsonic speeds. Additional work is needed to continue the validation of the computed results with the data and results from other techniques and extraction of the aerodynamic coefficients from the simulations at hand. The present CFD-RBD simulations clearly show the potential capability of the coupled approach and form the basis for future multidisciplinary, time-dependent computations of advanced maneuvering munitions.

5. References

1. Sahu, J.; Heavey, K. R.; Ferry, E. N. Computational Fluid Dynamics for Multiple Projectile Configurations. *Proceedings of the 3rd Overset Composite Grid and Solution Technology Symposium,* Los Alamos, NM, October 1996.

2. Sahu, J.; Heavey, K. R.; Nietubicz, C. J. Time-Dependent Navier-Stokes Computations for Submunitions in Relative Motion. *Sixth International Symposium on Computational Fluid Dynamics*, Lake Tahoe, NV, September 1995.

3. Meakin, R. L. *Computations of the Unsteady Flow About a Generic Wing/Pylon/Finned-Store Configuration*; AIAA 92-4568-CP; August 1992.

4. Smith, B. L.; Glezer, A. The Formation and Evolution of Synthetic Jets. *Physics of Fluids* **1998**, *10* (9).

5. Amitay, M.; Kibens, V.; Parekh, D.; Glezer, A. *The Dynamics of Flow Reattachment over a Thick Airfoil Controlled by Synthetic Jet Actuators*; AIAA Paper No. 99-1001; January 1999.

6. Amitay, M.; Smith, D. R.; Kibens, V.; Parekh, D.; Glezer, A. Aerodynamic Flow Control over an Unconventional Airfoil using Synthetic Jet Actuators. *AIAA Journal* **2001**, *39*, 361-370.

7. Davis, S. A.; Glezer, A. *The Manipulation of Large- and Small-Scales in Coaxial Jets using Synthetic Jet Actuators*; AIAA Paper No. 2000-0403; January 2000.

8. He, Y.; Kral, L. *Post-Stall Control on an Airfoil using Localized Jet Actuators*; AIAA Paper No. 2000-0408.

9. Lee, C. Y.; Goldstein, D. B. *Two-Dimensional Synthetic Jet Simulation*; AIAA Paper No. 2000-0406; January 2000.

10. Avancha, R.; Pletcher, R. H. *Large Eddy Simulation of the Turbulent Flow Past a Backward Facing Step*; AIAA Paper No. 2000-0542; January 2000.

11. Arunajatesan, S.; Sinha, N. *Towards Hybrid LES-RANS Computations of Cavity Flowfields*; AIAA Paper No. 2000-0401; January 2000.

12. Batten, P.; Goldberg, U.; Chakravarthy, S. *Sub-grid Turbulence Modeling for Unsteady Flow with Acoustic Resonance*; AIAA Paper 00-0473; 38th AIAA Aerospace Sciences Meeting, Reno, NV, January 2000.

13. Pulliam, T. H.; Steger, J. L. On Implicit Finite-Difference Simulations of Three-Dimensional Flow. *AIAA Journal* **February 1982**, *18* (2), pp. 159–167.

14. Peroomian, O.; Chakravarthy, S.; Goldberg, U. *A 'Grid-Transparent' Methodology for CFD*; AIAA Paper 97-07245; 1997.

15. Peroomian, O.; Chakravarthy, S.; Palaniswamy, S.; Goldberg, U. *Convergence Acceleration for Unified-Grid Formulation Using Preconditioned Implicit Relaxation*; AIAA Paper 98-0116; 1998.

16. Goldberg, U. C.; Peroomian, O.; Chakravarthy, S. A Wall-Distance-Free K-E Model With Enhanced Near-Wall Treatment. *ASME Journal of Fluids Engineering* **1998**, *120*, 457-462.

17. Rinehart, C.; McMichael, J. M.; Glezer, A. *Synthetic Jet-Based Lift Generation and Circulation Control on Axisymmetric Bodies*; AIAA Paper No. 2002-3168.

18. McMichael, J. GTRI, Private Communications.

19. Sahu, J. *Unsteady Numerical Simulations of Subsonic Flow over a Projectile with Jet Interaction*; AIAA Paper 2003-1352, Reno, NV, 6-9 January 2003.

20. Sahu, J. *Unsteady CFD Modeling of Aerodynamic Flow Control over a Spinning Body with Synthetic Jet*; AIAA Paper 2004-0747, Reno, NV, 5-8 January 2004.

21. Sahu, J. *Time-Accurate Numerical Prediction of Free Flight Aerodynamics of a Finned Projectile*; ARL-TR-3603; U.S. Army Research Laboratory: Aberdeen Proving Ground, MD, September 2005.

22. Arrow Tech Associates. ARFDAS Technical Manual. South Burlington, VT, 2001.

NO. OF COPIES	ORGANIZATION
1 (PDF ONLY)	DEFENSE TECHNICAL INFORMATION CTR DTIC OCA 8725 JOHN J KINGMAN RD STE 0944 FORT BELVOIR VA 22060-6218
1	US ARMY RSRCH DEV & ENGRG CMD SYSTEMS OF SYSTEMS INTEGRATION AMSRD SS T 6000 6TH ST STE 100 FORT BELVOIR VA 22060-5608
1	DIRECTOR US ARMY RESEARCH LAB IMNE ALC IMS 2800 POWDER MILL RD ADELPHI MD 20783-1197
1	DIRECTOR US ARMY RESEARCH LAB AMSRD ARL CI OK TL 2800 POWDER MILL RD ADELPHI MD 20783-1197
2	DIRECTOR US ARMY RESEARCH LAB AMSRD ARL CI OK T 2800 POWDER MILL RD ADELPHI MD 20783-1197
1	COMMANDER NAVAL SURFACE WARFARE CNTR ATTN CODE B40 DR W YANTA DAHLGREN VA 22448-5100
1	COMMANDER NAVAL SURFACE WARFARE CNTR ATTN CODE 420 DR A WARDLAW INDIAN HEAD MD 20640-5035
1	AIR FORCE ARMAMENT LAB ATTN AFATL/FXA DAVE BELK EGLIN AFB FL 32542-5434
3	COMMANDER US ARMY TACOM-ARDEC ATTN AMSTA AR FSF T J GRAU H HUDGINS W KOENIG BLDG 382 PICATINNY ARSENAL NJ 07806-5000

NO. OF COPIES	ORGANIZATION
1	COMMANDER US ARMY TACOM-ARDEC LOS/BLOS ATTN AMSTA AR CCH B P VALENTI BLDG 354 PICATINNY ARSENAL NJ 07806-5001
1	NAVAL AIR WARFARE CENTER ATTN DAVID FINDLAY MS 3 BLDG 2187 PATUXENT RIVER MD 20670
1	UNIV OF TEXAS AT ARLINGTON DEPT OF MECH AND AEROSPACE ENG ATTN DR J C DUTTON BOX 19018 500 W FIRST ST ARLINGTON TX 76019-0018
1	COMMANDER US ARMY TACOM-ARDEC ATTN AMCPM DS MO P BURKE BLDG 162S PICATINNY ARSENAL NJ 07806-5000
1	METACOMP TECH ATTN S CHAKRAVARTHY 28632B ROADSIDE DR STE 255 AGOURA HILLS CA 91301
1	AEROPREDICTION INC ATTN F MOORE 9449 GROVER DRIVE STE 201 KING GEORGE VA 22485
2	ATK TACTICAL SYSTEMS DIV ALLEGANY BALLISTICS LAB ATTN D J LEWIS J S OWENS 210 STATE ROUTE 956 ROCKET CENTER WV 26726
1	ATK ADVANCED WEAPONS DIV ATTN R H DOHRN MN06 1000 4600 NATHAN LANE N PLYMOUTH MN 55442
1	ATK ORDNANCE SYS ATTN B BECKER MN07 MW44 4700 NATHAN LANE NORTH PLYMOUTH MN 55442-2512

NO. OF COPIES	ORGANIZATION
1	SCIENCE APPLICATIONS INTL CORP ATTN J NORTHRUP 8500 NORMANDALE LAKE BLVD SUITE 1610 BLOOMINGTON MN 55437
3	GOODRICH ACTUATION SYSTEMS ATTN T KELLY P FRANZ J CHRISTIANA 100 PANTON ROAD VERGENNES VT 05491
3	ARROW TECH ASSOC ATTN W HATHAWAY J WHYTE MARK STEINOFF 1233 SHELBURNE RD STE D8 SOUTH BURLINGTON VT 05403
1	KLINE ENGINEERING CO INC ATTN R W KLINE 27 FREDON GREENDEL RD NEWTON NJ 07860-5213
3	GEORGIA INST TECH DEPT AEROSPACE ENGR ATTN M COSTELLO A GLEZER M ALLEN 270 FERST STREET ATLANTA GA 30332-0150
1	AIR FORCE RSRCH LAB ATTN AFRL/MNAV G ABATE 101 W EGLIN BLVD STE 333 EGLIN AFB FL 32542-6810
1	COMMANDER US ARMY ARDEC ATTN AMSRD AAR AEM A G MALEJKO PICATINNY ARSENAL NJ 07806-5000
1	COMMANDER US ARMY ARDEC ATTN ASMRD AAR AEP E D CARLUCCI PICATINNY ARSENAL NJ 07806-5000
1	COMMANDER US ARMY ARDEC ATTN ASMRD AAR AEP E C KESSLER PICATINNY ARSENAL NJ 07806-5000
1	COMMANDER US ARMY ARDEC ATTN ASMRD AAR AEP E I MEHMEDAGIC PICATINNY ARSENAL NJ 07806-5000

NO. OF COPIES	ORGANIZATION
1	PRODUCT MGR SMALL AND MED CALIBER AMMO ATTN SFAE AMO MAS SMC R KOWALSKI BLDG 354 PICATINNY ARSENAL NJ 07806
1	PM MAS ATTN SFAE AMO MAS PICATINNY ARSENAL NJ 07806-5000
1	PM CAS ATTN SFAE AMO CAS PICATINNY ARSENAL NJ 07806-5000
3	US ARMY AMRDEC ATTN AMSAM RD SS AT L AUMAN R W KRETZSHMAR E VAUGHN REDSTONE ARSENAL AL 35898-5000
1	COMMANDER US ARMY ARDEC ATTN AMSTA DSA SA A CLINE PICATINNY ARSENAL NJ 07806-5000
4	COMMANDER US ARMY ARDEC ATTN AMSRD AAR AEM I B 65N J STEINER R P MAZESKI D J DURKIN R MONTENEGRO PICATINNY ARSENAL NJ 07806-5000
2	DIRECTOR US ARMY RSCH LABORATORY ATTN AMSRD ARL RO EN T DOLIGALSKI AMSRD ARL RO P D MANN RSCH TRIANGLE PARK NC 27703
3	CDR USAMCOM ATTN AMSAM RD MG J BAUMANN J LOCKER AMSRD AMR SG SD B NOURSE REDSTONE ARSENAL AL 35898-5000
1	JOHNS HOPKINS APPL PHYSICS LAB ATTN DR WM D'AMICO 11100 JOHNS HOPKINS ROAD LAUREL MD 20723-6099
1	PM MAS ATTN SFAE GCSS ARMS G DEROSA BLDG 171A PICATINNY ARSENAL NJ 07806-5000

NO. OF COPIES	ORGANIZATION
4	GEORGIA TECH RSCH INST ATTN J MCMICHAEL K MASSEY A LOVAS M HEIGES 7220 RICHARDSON ROAD SMYRNA GA 30080
2	DARPA/TTO ATTN DR S WELBY DR S WALKER 3701 NORTH FAIRFAX DR ARLINGTON VA 22203-1714
1	AIR FORCE WRIGHT LAB ATTN AFATL/FXA D BELK 101 W EGLIN BLVD EGLIN AFB FL 32542
3	BAE SYSTEMS ATTN R BURETTA CODE 170 B GOODELL J QUINN 4800 EAST RIVER ROAD MINNEAPOLIS MN 55421
	ABERDEEN PROVING GROUND
1	DIRECTOR US ARMY RSCH LABORATORY ATTN AMSRD ARL CI OK (TECH LIB) BLDG 4600
1	DIR USARL AMSRD ARL CI H C NIETUBICZ BLDG 328
18	DIR USARL AMSRD ARL WM J SMITH AMSRD ARL WM B M ZOLTOSKI AMSRD ARL WM BA D LYON AMSRD ARL WM BC P PLOSTINS J DESPIRITO B GUIDOS K HEAVEY J NEWILL J SAHU (2 CYS) S SILTON P WEINACHT M CHEN X HUANG G COOPER AMSRD ARL WM BD B FORCH AMSRD ARL WM BF S WILKERSON AMSRD ARL WM EG E SCHMIDT

1 JOHN A EDWARDS
DSTL FELLOW
MCM DEPARTMENT
DSTL FORT HALSTEAD
SEVENOAKS
KENT NT14 7BP UK